Near to far field correlation of crackle-related events in military aircraft jet noise

Aaron B. Vaughn, Kent L. Gee, Kevin M. Leete, et al.

Citation: Proc. Mtgs. Acoust. **42**, 045008 (2020); doi: 10.1121/2.0001442
View online: https://doi.org/10.1121/2.0001442
View Table of Contents: https://asa.scitation.org/toc/pma/42/1
Published by the Acoustical Society of America

Volume 42 http://acousticalsociety.org/

179th Meeting of the Acoustical Society of America

Acoustics Virtually Everywhere

7-11 December 2020

Physical Acoustics: Paper 3aPAc1

Near to far field correlation of crackle-related events in military aircraft jet noise

Aaron B. Vaughn, Kent L. Gee and Kevin M. Leete
Department of Physics and Astronomy, Brigham Young University, Provo, UT, 84602; aaron.burton.vaughn@gmail.com; kentgee@byu.edu, kevinmatthewleete@gmail.com

J. Micah Downing
Blue Ridge Research and Consulting LLC, Asheville, NC, 28801; micah.downing@blueridgeresearch.com

Crackle perception in supersonic jet noise is attributed to the presence of acoustic shocks in the waveform. This study uses an event-based beamforming method to track shock events as they propagate from the near to the far field of a high-performance military aircraft operating at afterburner. Near-field events are propagated via a nonlinear model and compared with far-field measurements. Comparisons of overall sound pressure level and spectra validate the use of the nonlinear model. The skewness of the time-derivative pressure waveform, or derivative skewness, a metric indicative of jet crackle perception, is greatly overpredicted for nonlinearly propagated waveforms. Cross-correlation coefficients of waveform segments centered about the near-field beamformed events reveal that for farther aft angles, near-field events are more related to far-field measurements. Waveform observations show that shock-like events in the near field that are more spiked in nature tend not propagate into the far field. However, near-field, large-derivative events with broader, high-pressure peaks nonlinearly steepen and form shocks in the far field that are likely responsible for crackle perception.

Published by the Acoustical Society of America

 https://doi.org/10.1121/2.0001442

1. INTRODUCTION

Jet crackle is an annoying[1] and dominant[2] component of supersonic jet noise. As a potential factor in community annoyance, crackle depends on the existence of shocks in the far field. Shocks may exist at far-field locations due to nonlinear propagation of large-amplitude waveforms that steepen with distance or the persistence of near-field shocks into the far field. A recent jet noise study of a tethered high-performance military aircraft investigated the source of crackle-related events measured in the near field.[3] Follow-on research further investigated those events and determined a significant number of them to be shocks.[4] The objective of the present study is to investigate the relationship between near-field events and far-field measurements correlated with crackle perception. This study employs a nonlinear model to propagate waveforms collected at a near-field ground array into the far field to compare with far-field measurements.

There is some debate as to whether crackle is a propagation or source phenomenon. In the initial crackle study, Ffowcs Williams *et al*.[1] suggested that crackle was a source phenomenon. This claim is supported by the use of the pressure skewness as an indicator for crackle perception, as pressure skewness decays with distance from the source. However, Gee *et al*.[5] showed that the skewness of the time-derivative of the pressure waveform, or derivative skewness, is strongly correlated to crackle perception while the pressure skewness is not. Furthermore, Gee *et al*.[6] have shown that large-amplitude waveforms produced near an F-35 nonlinearly propagate, causing waveforms to steepen and form shocks, which subsequently increases the derivative skewness with distance, until the waveforms and shocks substantially decay.[7] Derivative skewness is a better metric for crackle perception prediction than the pressure skewness, as the pressure skewness decays with distance and does not vary with shock formation, as does the derivative skewness.[8,9]

In order to make comparisons between the near-field crackle-related events and far-field measurements, waveforms need to be propagated using a nonlinear method. Early observations by Morfey and Howell[10] of flyover measurements of the Concorde (the same aircraft studied by Ffowcs Williams *et al*.[1]) and other high-power aircraft suggested a nonlinear model over a linear one to predict jet noise propagation. A linear model generally assumes significant high-frequency attenuation due to atmospheric absorption; however, Morfey and Howell[10] observed greater high-frequency energy than explained by linear models. This irregularity is rectified by a nonlinear energy transfer to high frequencies as explained in a nonlinear model. The nonlinear model used in this study is the generalized Burgers equation (GBE). The GBE is a partial differential equation that accounts for an amplitude-dependent sound speed, which causes waveform steepening: large positive peaks in the waveform travel faster while large negative pressure peaks (relative to ambient pressure) travel slower. Intermediate engine powers and greater are expected to have sufficient conditions for waveforms to experience significant nonlinear steepening, as has been validated for several aircraft.[11–13] Other uses of this same nonlinear model include a plane-wave tube study[14] and rocket noise.[15]

The primary analysis performed to compare propagated, near-field events with far-field measurements utilizes cross-correlation coefficients. Previously, a variety of correlation analyses have been implemented to characterize near-field jet noise sources.[16–19] This study, however, seeks to use correlation as a means to relate the results of the crackle-related source localization to far-field measurements. Near-field waveforms are propagated numerically via the GBE, then cross-correlation coefficients are calculated for large number of individual events, which are the same events identified and examined in Ref. 3.

The study contained in this paper compares nonlinearly propagating waveforms collected in the near field with far-field measurements for the F-35B operating at 150% engine thrust request (ETR). This engine power was selected because nonlinear propagation effects are expected to be the greatest. Relevant measurement information can be found in Refs. 3, 4, and 20. A brief description of the nonlinear model along with the process for selecting waveforms and events to compare with far-field measurements are provided. Validation of the nonlinear model is made using comparisons between the OASPL, derivative skewness, and spectra for the nonlinear propagated and measured waveforms. An analysis using cross-correlation coefficients of comparable waveform segments is made to quantify the relationship between propagated and measured waveforms, after which a concluding discussion is given.

2. NEAR TO FAR-FIELD CORRELATION METHODS

A description of the nonlinear model using the GBE is first provided. Then the process is given for determining the waveform segment to nonlinearly propagate to compare with overall far-field trends. A subset of eight microphones are selected for more direct comparisons between propagated and measured waveforms. Lastly, the method for calculating cross-correlation coefficients for individual events is provided.

A. NONLINEAR MODEL

Selected waveform segments are propagated using a nonlinear propagation model based on the generalized-Burger's equation (GBE) that incorporates cumulative quadratic nonlinearity, atmospheric absorption and dispersion, and spherical spreading as found in Ref. 12. This formulation of the GBE in a retarded time frame is as follows:

$$\frac{\partial p}{\partial r} = \frac{\beta}{2\rho_0 c_0^3}\frac{\partial p^2}{\partial \tau} + \psi_\tau\{p\} - \frac{1}{r}p \qquad \textbf{(1)}$$

where $p(r,\tau)$ is the acoustic pressure, r is the output distance, τ is the retarded time of propagation between the input distance and r, β is the coefficient of nonlinearity, ρ_0 is the ambient air density, c_0 is the ambient speed of sound, and ψ_τ is an operator representing atmospheric absorption and dispersion that acts on $p(r,\tau)$. Equation (1) is solved incrementally using a time-frequency domain algorithm that is based on methods in Refs. 21 and 22 and described in more detail in Refs. 12, 13 and 23.

B. WAVEFORM SELECTION PROCESS

Results from the source localization of crackle-related events in Ref. 3 are used to identify angles at which to propagate near-field measurements into the far field. Initial comparisons between nonlinearly propagated waveforms and far-field measurements are made using all 70 microphone pairs along the ground array. Figure 1 shows the outward ray tracings of the propagation angle modes for 150% ETR. These rays are extrapolations of the inward ray tracings shown in Figure 10d of Ref. 3. Upstream radiation of group 1 (blue) is of less interest in the near field because of low derivative skewness values but can have appreciable growth in the forward direction.[7] Most outward ray tracings range from 110º to 150º. This region is of interest because derivative skewness values are sufficient for crackle perception along the 305 m arc, as established in a previous crackle listening study.[5,20,24] Angles relative to the microphone array reference point (MARP) at which the outward ray tracings intersect with the microphone arcs are used as their position for comparisons of the OASPL and derivative skewness values with the measured data. Waveforms are numerically propagated at 204.8 kHz, which was the sampling frequency at the near-field array, then downsampled to 96 kHz for comparison with far-field measurements.

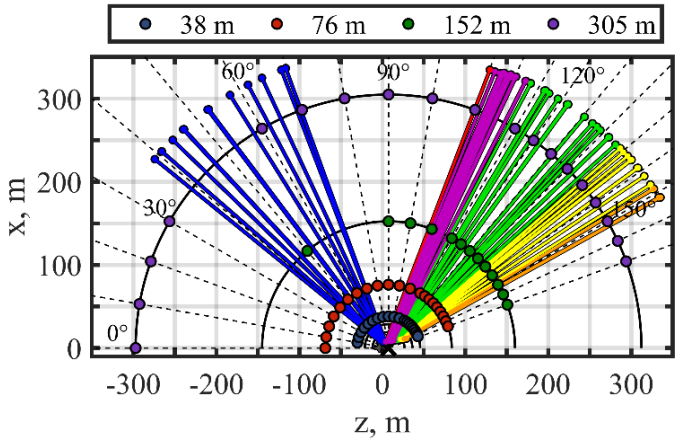

Figure 1 Outward ray tracings of the propagation angle mode from the event-based beamforming for 150% ETR (see Figure 10d in Ref. 3 for inward ray tracing for inward ray tracing).

I. EVENT SELECTION

The same 1000 largest derivative events used in the source localization study in Ref. 3 are defined in the 36-s waveforms. For simplicity, a 20.48-s segment is chosen to be nonlinearly propagated and compared with the far-field measurements. On average, the 20.48-s segment contains ~750 large derivative events. An iterative process is used to find a 20.48-s segment with similar OASPL and derivative skewness values to that of the overall waveform. Across the entire array, derivative skewness values for a 5.12-s segment may vary by as much as 10% while the OASPL varies less than 1 dB compared to the 36-s waveform.

II. MICROPHONE SUBSET SELECTION

Ideal ground array measurements to compare directly with far-field measurements are those that have events projected to propagate near microphones along far-field arcs. A subset of eight microphones along the ground array are used to compare waveform segments centered about previously beamformed events using cross-correlation coefficients. Information for the locations, associated event-based beamforming group as defined in Ref. 3, propagation angles, and intersection angles with radial arcs are given in Table 1. Due to the sparseness of far-field arc microphones every 5º or 10º, ground array microphones were chosen with events that have propagation angle modes such that the outward traced rays intersect near locations of far-field microphones. This generally means that the ground array microphones selected fall along a jet inlet angle radial as defined by the MARP and have similar propagation angle to the radial angle. The normalized histogram distributions in Figure 6b of Ref. 3 show that microphone pairs with events that propagate 110º to 150º have a spread of about 10°, which helps justify the use of the mode and splitting the difference of intersection angles across the arcs.

Table 1 Radial angles of interest, event-based beamforming group number and color, propagation angle modes, array position jet inlet angle, and the intersection angle with far-field arcs for the subset of eight ground array microphones used in the near to far-field event comparison.

Radial Angle	Group Number (& Color)	Propagation Angle Mode	Array Position Angle	19 m	29 m	38 m	76 m	152 m	305 m
110°	3 (Purple)	113°	104.0°	108.9°	110.2°	110.9°	112.0°	112.5°	112.7°
120°	4 (Green)	118°	127.3°	123.7°	121.8°	120.9°	119.4°	118.7°	118.4°
125°	4 (Green)	124°	131.6°	-	-	126.5°	125.3°	124.6°	124.3°
130°	4 (Green)	130°	138.4°	-	-	133.3°	131.6°	130.8°	130.4°
135°	4 (Green)	134°	140.2°	139.1°	137.6°	136.6°	135.3°	134.6°	134.3°
140°	5 (Yellow)	139°	144.0°	-	-	141.3°	140.2°	139.6°	139.3°
145°	5 (Yellow)	144°	147.1°	-	-	145.6°	144.8°	144.4°	144.2°
150°	6 (Orange)	149°	150.4°	-	-	150.4°	150.7°	150.9°	150.9°

A smaller subset of three of the eight microphones in Table 1 are used to examine waveform features in Section C. While the outer four arcs (38 to 305 m) are of primary interest because of their position in the far field, two additional inner arcs at $r = 19$ m and 28 m have microphones at a more limited number of positions. For 110°, 120°, and 135°, microphones exist at both the inner 19 and 29 m arcs, whereas microphones only exist at one or neither location for other angles. This allows for a more incremental comparison between the nonlinearly propagated and measured waveforms in Section C and their corresponding cross-correlation coefficients in Section D.

C. CROSS-CORRELATION COEFFICIENTS

Near-field, crackle-related events are directly compared to far-field measurements using cross-correlation coefficients. First, to time-align waveforms, a cross-correlation is performed to find a time lag between the 20.48-s propagated waveform segment given in retarded time and the measured waveform at the propagated distance. Similar time-alignment can be found using the measured distances and speed of sound with differences of less than 0.1 ms up to the 76 m arc and within a few milliseconds at the 152 and 305 m arcs. Discrepancies are expected to increase with distance, as the assumed pathlength may differ due to microphone position uncertainty, varying ambient conditions impacting the speed of sound, wind, and the directivity of the beamformed events being different from that of the overall energy in the waveform. After waveforms are temporally aligned, cross-correlation coefficients, ρ_{xy}, are calculated for the entire 20.48-s waveform and each individual event. For each of the ~750 large-derivative events of interest, the 10-ms waveform segment centered about the event in the propagated and measured waveforms is used to calculate ρ_{xy}. While no windowing or variable segment length based on the characteristic frequency of the waveform is applied, these could be done to improve results.[16] The ρ_{xy} values are found only using nonlinear propagation on the ground-array waveform, which does not account for meteorological, terrain, or other measurement effects.

3. RESULTS AND ANALYSES

Validation and limitations of the nonlinear model are examined by comparing measured and propagated OASPL, derivative skewness, and spectra in Sections A and B. Example waveforms are examined in Section C for three radial cases to provide a qualitative comparison of near to far-field crackle-related events. Lastly, cross-correlation coefficients for the propagated and measured shock waveforms segments are compared, providing a quantitative relationship between near and far-field events in Section D.

A. OASPL AND DERIVATIVE SKEWNESS COMPARISON

Comparisons between propagated and measured of OASPL and derivative skewness along four arcs are shown in Figure 2. Each plot denotes for a given arc array the measured values in black and the values of the propagated waveforms in colors, which represent the color groupings from Ref. 3. Groups 3, 4, and 5 (purple, green, and yellow) are related to crackle perception at the near-field ground array, while the others are not, though their derivative skewness values may increase sufficiently for crackle perception in the far field.

The OASPL and derivative skewness have similar trends for both the propagated and measured data. The OASPL and derivative skewness for the propagated waveforms peak at larger angles. This suggests that the directivity of the noise source responsible for the large derivative events for those groups may be fundamentally different than the directivity of the noise components producing the majority of the time-averaged energy. This region where the levels and derivative skewness are greater correspond primarily to group 5 (yellow), for which there is a slight increase in OASPL in the near field that perhaps does not radiate efficiently into the far field. Despite the disparity between directivities and peak values, the nonlinear propagation produces waveforms similar to the measured values in the far field.

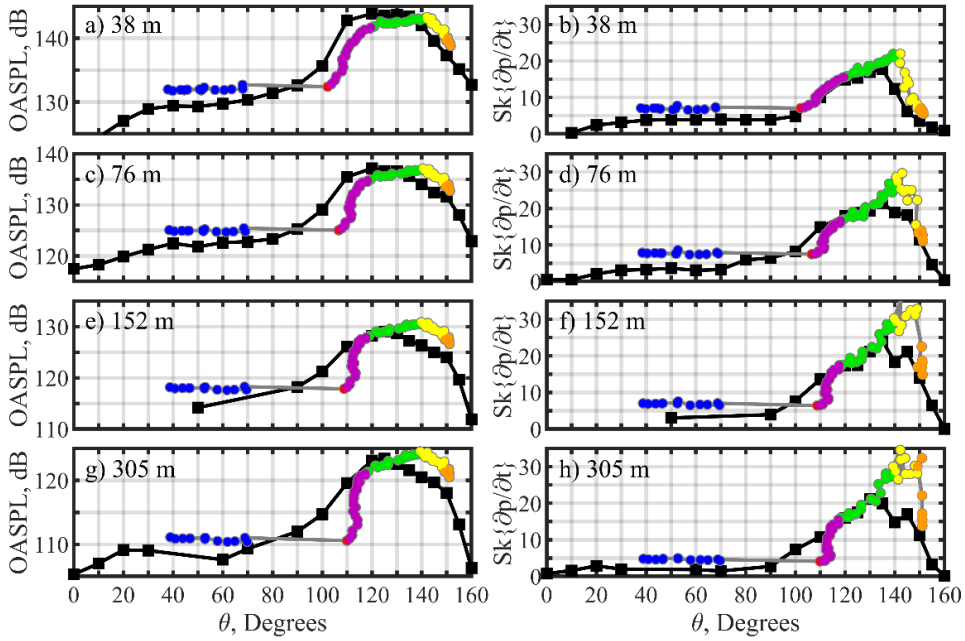

Figure 2 Measured and nonlinearly propagated projected OASPL and derivative skewness along the a) b) 38 m, c) d) 76 m, e) f) 152 m, and g) h) 305 m arcs. Colors identify event-based beamforming group, as defined in Ref. 3.

The choice of spherical spreading in the nonlinear model appears appropriate as validated by OASPL trends as a function of distance. For select angles from Table 1, OASPL and derivative skewness values as a function of distance are shown in Figure 3. The spherical decay rate, η, as a function of distance, r, is given as:

$$\eta = 20\log_{10}\left(\frac{1}{r}\right) \quad \textbf{(2)}$$

and is denoted by the blue dashed line in Figure 3. There is a 150-dB offset applied to η allow for comparison with measured and propagated levels. Generally, the measured and propagated levels follow the spherical decay rate. The propagated waveforms' OASPL are slightly underpredicted at some locations for 110° and 120° and overpredicted at 140° and 150°. Some reasons for discrepancies in levels could include near-field measurements

capturing noise that does not radiate spherically at those distances, different directivity for the beamformed events from the overall average waveform energy, terrain, meteorological, and other measurement effects. Despite the discrepancies due to proposed and other reasons, the resulting OASPL reasonably follow spherical decay.

The derivative skewness in Figure 3 reveals limitations in making direct comparisons using the derivative skewness values between the measured and propagated waveforms in the far field. The first derivative skewness point, representing the value measured at the ground array, is consistently greater than the value at the nearest arc measurement, which are located 5′ off the ground. This is likely attributed to the presence of nonlinear reflections occurring at the ground measurements, as discussed in Ref. 4. Despite this discrepancy, the derivative skewness values approach nearly identical values by the 305 m arc for 130° and lower angles. Contrarily, at 140° and 150° the derivative skewness for the propagated waveforms are consistently greater. At 140°, both the propagated and measured waveforms follow a similar spatial derivative skewness trend of increasing then decreasing with distance, despite the discrepancy in values. A similar trend is observed up to the 152 m arc for 150°, but the derivative skewness continues to increase to the 305 m arc for the propagated waveform while the measured value decreases. The greater levels at 140° and 150° suggest that there is a larger potential for large-pressure events at the ground array to form into shocks with propagation. However, despite physical limitations of the nonlinear model, reasonable results are produced.

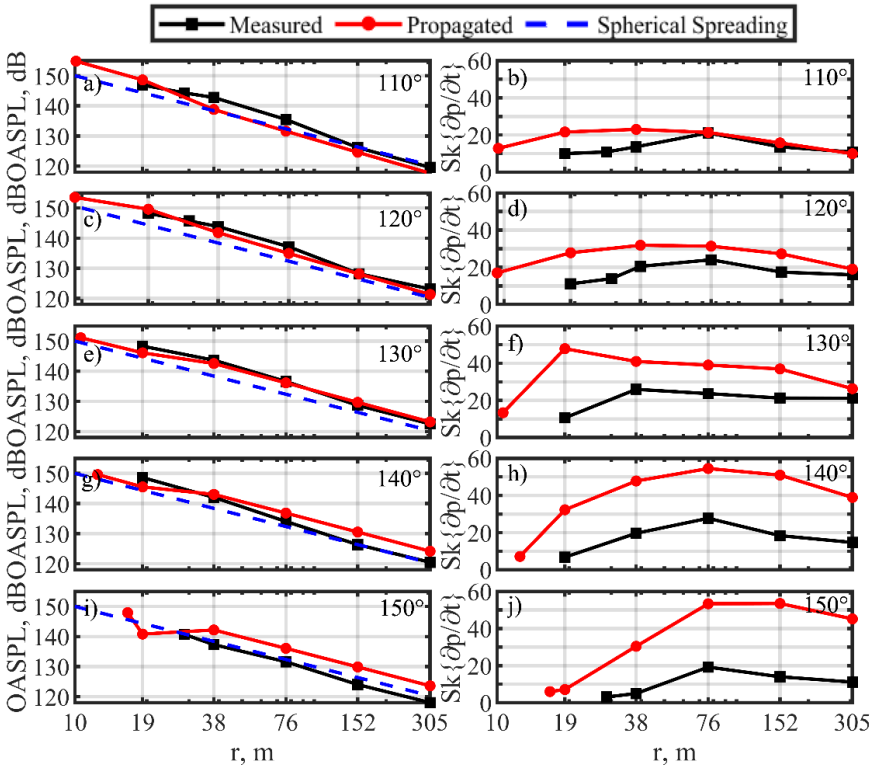

Figure 3 Measured and nonlinearly propagated a) OASPL and b) derivative skewness values along the 110° radial, c) OASPL and d) derivative skewness along the 120° radial, e) OASPL and f) derivative skewness along the 130° radial, g) OASPL and h) derivative skewness along the 140° radial, andic) OASPL and j) derivative skewness along the 150° radial. The blue dashed line in the OASPL plots represents spherical decay.

B. SPECTRAL COMPARISON

Spectral comparisons further validate the nonlinear model. Figure 4 shows spectral comparisons between the propagated (red) and measured (black) for the same waveforms examined in Figure 3 with the propagated angles reported in Table 1. Each row represents a different arc, while columns denotes a radial angle. For nearly all cases, high frequencies (>1 kHz) match well, which validates the use of the nonlinear model. Without the nonlinear model, the high frequencies would decay more rapidly and be underpredicted. Along the 38 m arc, the peak frequency is similar for both the measured and propagated waveform spectra, with 110° underpredicting the level, 150° overpredicting the level, and 120° to 140° nearly identical levels. As a function of distance, the

peak frequencies are higher for the propagated waveform spectra than the measured spectra in all cases at greater distances, while the levels are underpredicted for 110° and 120° and overpredicted for 140° and 150°. Along the 120° radial, the double peak in the propagated spectra matches well at the nearer two arcs, but the higher frequency peak decreases in level, becoming almost indistinguishable in the measured spectra at 152 m. Overall, despite the discrepancies about the peak, which further informs the differences observed for OASPL, the propagated and measured spectra match well, especially the high-frequency content.

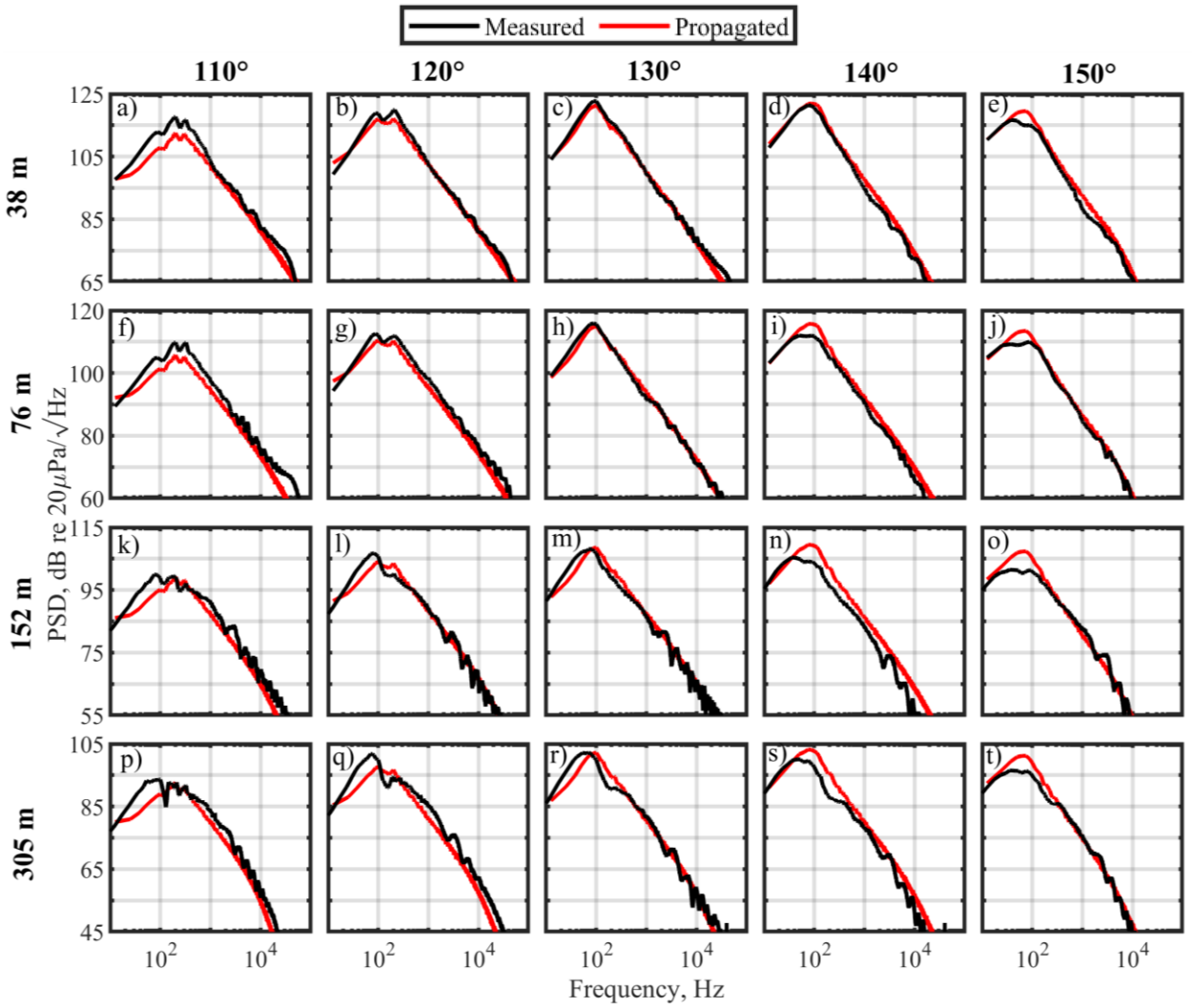

Figure 4 Spectra comparison between the measured (black) and nonlinearly propagated (red) waveforms. Columns refer to angles and rows represent radial arcs, as noted.

C. WAVEFORM COMPARISON

Example waveforms comparing propagated and measured shocks at six distances along three radials are examined in this section. The radial angles are 110°, 120°, and 135°. Information regarding the propagation waveform angles and their intersection angles with each far-field arc radial are in Table 1. Waveform segments of 20-ms length are shown for 19, 29, 38, 76, 152, and 305 m arc radials and compared with the corresponding measurements along the arcs. Each waveform is centered about a large derivative event denoted by a red x in the ground-array waveform in Figure 5a, 5b, and 7a. Other large-derivative events, that are considered shocks according to the $15\sigma_{\partial p/\partial t}$ shock criterion, may also exist within the 20-ms waveform and are similarly noted by a red x. Cross-correlation coefficients, ρ_{xy}, are calculated and reported for 10-ms segments centered about the main large derivative event at 0 ms (from -5 ms to 5 ms).

As shown in Figure 5, some shocks in the 20-ms waveform along the 110° radial (see row 1 in Table 1) do not persist to the far-field. The first large-derivative event at -8 ms in Figure 5a is more impulsive, with a more

abrupt rise and sharp drop after peaking, compared to the second event at 0 ms. As a function of distance, the first event decays rapidly and is nearly unidentifiable beyond the ground array in the measured waveforms, though it persists slightly in the propagated waveforms. Similarly, the narrow-peaked, shock-like event at about -5.5 ms also decays and is not readily identifiable beyond the ground array. There are also a number of small shocks throughout the measured 19 m arc waveform that do not persist into the far field.

There are near-field shock events that do propagate into the far field, as demonstrated by the central event at 0 ms. At the 19 m arc, the measured waveform still has not quite steepened into a single shock. Two factors that likely attribute to the lack of a formed shock at 19 m is that the shock identified in the ground array data (Figure 5a) is present in the off-ground data (Figure 5c) with a ground reflection and the shock measured at the ground could potentially be overly steepened due to the occurrence of an irregular shock reflection, as discussed in Ref. 4. As a result of the shock being fully formed at the ground, the derivative skewness at the ground is likely elevated and the subsequently propagated waveform decays more rapidly than the measured waveform, as there is increased absorption of energy at the shock peak. The behavior of the propagated versus measured waveforms can also be described by ρ_{xy}. The ρ_{xy} is lower at 19 m than 29 m, likely due to more significant ground interference at 19 m. Beyond 29 m, ρ_{xy} decreases with distance, partly due to shock being well formed at the ground, which decays more rapidly with distance relative to other waveform segments. At the 305 m arc, even though the propagated waveform does not ideally match the measurement, there is a shock present at 0 ms for the measured waveform, demonstrating that this event identified at the ground array persists into the far field.

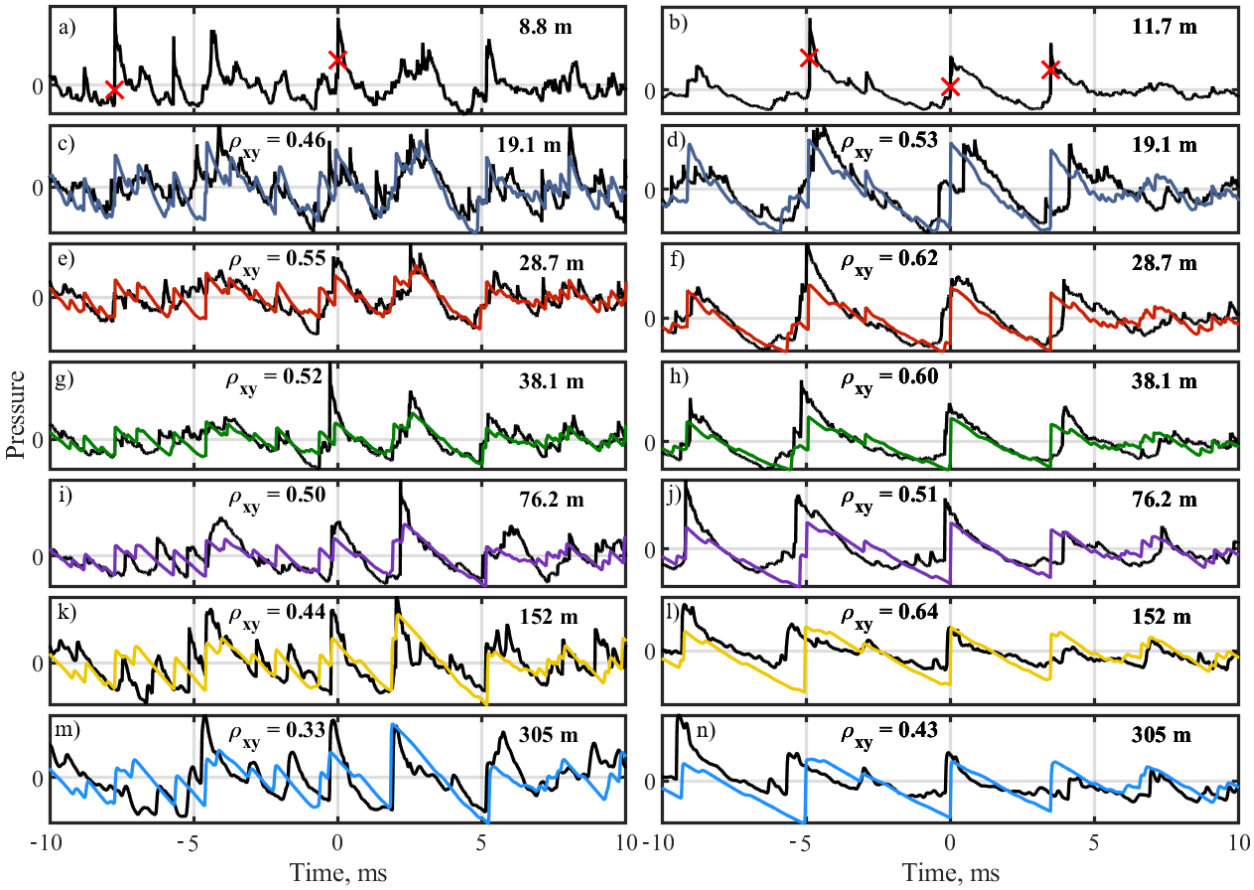

Figure 5 Example waveforms along the 110° (left) and 120° (right) radials at a–b) ground array and c–d) 19 m, e–f) 29 m, g–h) 38 m, i–j) 76 m, k–l) 152, and m–n) 305 m arcs. Black lines denote measured waveforms while colors represent the nonlinearly propagated waveforms. Cross-correlation coefficients for the 5-ms to 15-ms segment are also noted.

There are other near-field events that give rise to far-field shocks. Another significant shock exists at about 2 ms in Figure 5m for both waveforms at the 305 m arc, though it does not originate as a shock at the ground array. From about 2 to 4 ms in the ground-array waveform in Figure 5a, there is a broad, large pressure waveform

segment. This progressively steepens to form a distinct shock by 76 m. From these examples, it is observed that not all large-derivative shock events necessarily propagate into the far field, and large pressure events may also have the potential to form far-field shocks.

The persistence of first and second shocks and decline of the third shock into the far field are observed in the waveform example along the 120° radial, also shown in Figure 5. The first shock at -5 ms is the narrowest in peak and decays more rapidly than the measured waveforms at each radial distance. The second event occurs at the waveform center (0 ms) and is most similar to the measured waveform along all the arcs. The ground reflection is pronounced at 19 m, which again causes ρ_{xy} to be lower than at 29 m. Similar to 110°, ρ_{xy} generally decreases with distance for 120°, though it increases slightly at the 152 m arc. The third defined event at about 3.5 ms is more similar to the event at -5 ms in Figure 5bthan the second event, and subsequently the nonlinear propagation scheme causes it to decay and underpredict the peak up to 38 m, then it actually overpredicts at farther arcs. Time misalignment for the first and third events are probably due to the shocks having slightly different propagation angles relative to the assumed mode value.

More distinct and stronger correlated events are observed at farther aft locations. Compared to 110° and 120°, the large derivative event in the waveform propagated along the 135° radial is more isolated, with a single shock forming in the 20-ms waveform shown in Figure 6. The ρ_{xy} values are greatest for this of the three radials, with the 10-ms segment focused only on the event of interest. A window or more limited waveform segment based on the characteristic frequency of the waveform for the 110° and 120° cases may allow for more direct comparison between propagated and measured events using ρ_{xy} values. Despite the slight mismatch about the peak and the underpredicted pressures before the shock, the propagated and measured waveforms appear quite similar up to 38 m and somewhat similar at greater distances.

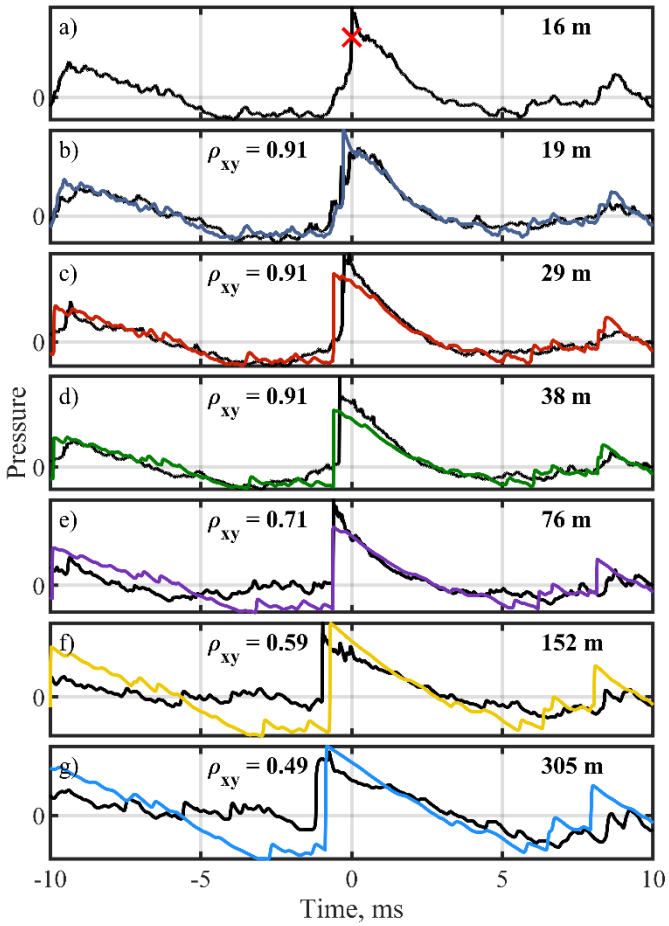

Figure 6 Example waveforms along the 135° radial at a) ground array and b) 19 m, c) 29 m, d) 38 m, e) 76 m, f) 152, and g) 305 m arcs. Black lines denote measured waveforms while colors represent the nonlinearly propagated waveforms. Cross-correlation coefficients for the 5-ms to 15-ms segment are also noted.

D. CROSS-CORRELATION COEFFICIENT HISTOGRAMS

Cross-correlation coefficients, ρ_{xy}, are calculated for segments of propagated and measured waveforms centered about shock events to provide a quantitative relationship of near-field crackle-related events and far-field measurements. The distribution of calculated ρ_{xy} values for the 10-ms waveform segments centered about each of the ~750 event are presented as box and whisker plots. Corresponding to the waveforms examined in Section C, ρ_{xy} distributions for six distances are first compared for three angles in Figure 7. Only the outer four arcs (38, 76, 152, and 305 m) are considered for the ρ_{xy} distributions of eight angles in Figure 8. For each distribution, the bottom and top edges of the box indicate the 25th and 75th percentiles, respectively, while the central mark notes the median. The whiskers extend to approximately $\pm$ 2.7 σ and 99.3% coverage assuming the data are normally distributed, with outliers are noted by red pluses. Lastly, comparisons between the ρ_{xy} value of the 20.48-s waveforms and the medians of the ρ_{xy} distributions for the event comparisons are given in Table 2, revealing the significance of the ρ_{xy} values of the propagated events in the far field.

Spatially, the ρ_{xy} values are greater at farther aft angles and decreases with increased propagation distance. Distributions of ρ_{xy} values are presented in Figure 7 for the six distances at the three angles that waveform examples were previously provided for in Section C. Parts a) through c) are respectively for 110°, 120°, and 135° with each box-whisker corresponding to the distribution of ρ_{xy} values for the 750 propagated events compared at a particular arc. Comparing across angles, distribution of ρ_{xy} values increases from 110° to 120° to 135°. With shocks occurring in quicker succession at 110°, they have more of a potential impact on affecting the cross-correlation about the events of interest. A window or a shorter waveform segment at lower angles may help to focus on just comparing the event itself, as Harker *et al.*[16] suggests temporal normalization to more meaningfully compare correlations at different angles. Similar to previously examined waveforms of individual events, the ρ_{xy} distributions decrease as a function of distance. The ρ_{xy} values are generally greater at the 29 m than 19 m arc, likely due to ground reflections decreasing the correlation between the propagated ground waveform and the off-ground measurement along the 19 m arc. Despite the increase from 19 to 29 m, ρ_{xy} generally decreases with greater propagation distance, as the physical effects not incorporated into the nonlinear propagation model potentially have a greater impact.

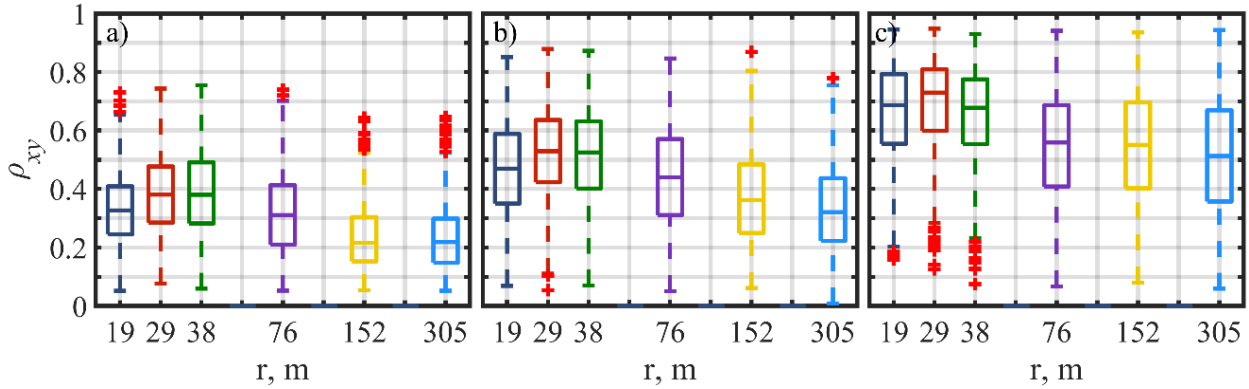

Figure 7 Box and whisker plots of cross-correlation coefficients distribution for the 750 propagated events compared with measured waveforms for the 6 arcs (19, 29, 38, 76, 152, and 305 m) along the a) 110°, b) 120°, and c) 135° radials. On each box, lower and upper edges respectively represent the 25th and 75th percentiles with central line indicating the median. The whiskers extend to the most extreme values not considered outliers, while outliers noted as red pluses.

Similar spatial trends are observed for ρ_{xy} values in Figure 8. Instead of each subplot corresponding to an angle, they now represent an arc, ranging from 38 to 305 m, and box-whiskers are distributions for a given angle along the arc. A quick visual inspection of Figure 7 shows the angular trend of ρ_{xy} values increasing with angle, while Figure 8 demonstrates the decrease of ρ_{xy} values increasing with distance. With more angles present in Figure 8, an increase in increasing ρ_{xy} values with angle is observed from 110° to 130°, while 130° to 150° perform almost equally well.

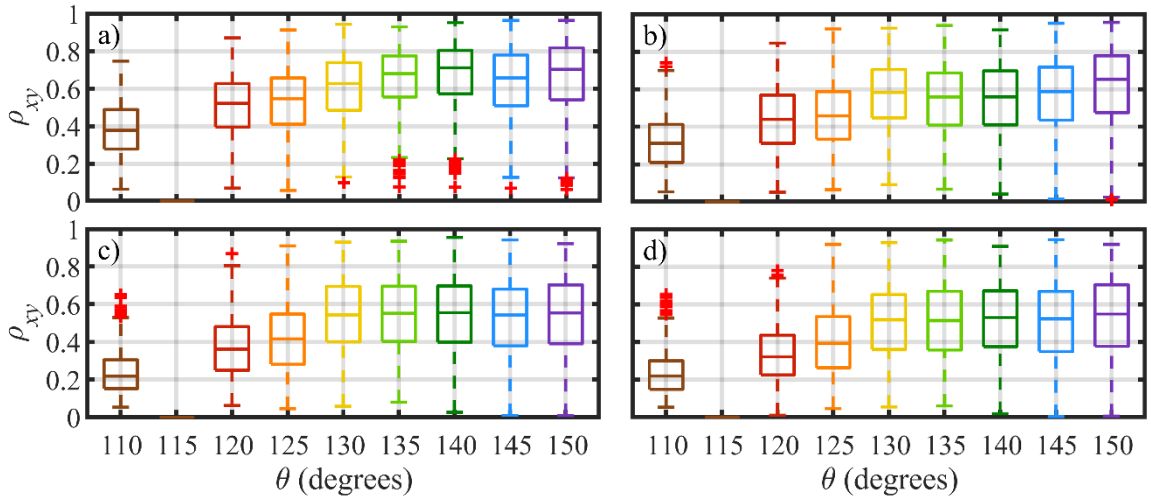

Figure 8 Box and whisker plots of cross-correlation coefficients distribution for the 750 propagated events compared with measured waveforms for angles ranging from 110 to 150° along the a) 38, b) 76, c) 152, and d) 305 m arcs. On each box, lower and upper edges respectively represent the 25th and 75th percentiles with central line indicating the median. The whiskers extend to the most extreme values not considered outliers, while outliers noted as red pluses.

To provide a reference to the significance of the ρ_{xy} distributions of the compared propagated events with far-field measurements, ρ_{xy} values of the entire 20.48-s waveforms and for the median of event comparison distribution are listed in Table 2. The ρ_{xy} value for the comparison of the 20.48-s propagated waveform and far-field measured waveform is noted in Table 2 as "waveform" and the median of the ρ_{xy} distribution of the 750 propagated events compared with far-field measurements in 10-ms segments as "events." The ρ_{xy} value is consistently lower for the waveform than the events. Over half of the events for 130° to 150° have $0.5 > \rho_{xy}$. These distributions serve to show that there are a significant number of events from the near field that are related to waveform segments in the far field. However, these results do not directly answer how many of these events are directly responsible for crackle perception in the far field. From the waveform examples in Section C, shocks measured in the near field may persist into the far field and result in large ρ_{xy} values, while others do not. Regardless, there is a significant correlation between the near-field crackle-related events and measurements in the far field.

Table 2 Cross-correlation values for the 20.48 s waveforms and the median for the event distribution shown in Figure 8 for the four arcs and eight angles represented in Table 1.

Angle	38 m Arc		76 m Arc		152 m Arc		305 m Arc	
	Waveform	Events	Waveform	Events	Waveform	Events	Waveform	Events
110°	0.29	0.36	0.18	0.28	0.05	0.19	0.04	0.19
120°	0.41	0.52	0.31	0.44	0.12	0.39	0.09	0.32
125°	0.48	0.55	0.39	0.48	0.16	0.42	0.15	0.42
130°	0.56	0.64	0.52	0.58	0.23	0.57	0.20	0.53
135°	0.64	0.67	0.47	0.56	0.22	0.55	0.20	0.51
140°	0.68	0.72	0.49	0.58	0.23	0.56	0.21	0.53
145°	0.55	0.68	0.47	0.58	0.20	0.55	0.18	0.52
150°	0.60	0.69	0.55	0.61	0.20	0.55	0.18	0.52

4. CONCLUSION

Near-field, event-based beamforming results have been extrapolated using a nonlinear model based on the GBE and compared to far-field measurements. Some limitations to the nonlinear model are that it does not include reflections, terrain effects, ray tracing due to wind or temperature gradients, and the input not necessarily being in the geometric far field where the spreading is most appropriately represented as spherical. The GBE

assumes spherical spreading, quasi-one-dimensional propagation, quiescent neutral atmosphere, atmospheric absorption and dispersion, and quadratic nonlinearity. Despite these limitations of the nonlinear model, it performs sufficiently well to produce meaningful comparisons of near-field events and far-field measurements. Validation of the nonlinear model include propagated and measured OASPL following a similar trend to spherical decay with distance and propagated and measured spectra matching at high-frequencies with a 20-dB decay per decade as expected for nonlinear propagation. Similar OASPL and derivative skewness values were found for both the propagated and measured data, though the directivity of the propagated OASPL and derivative skewness were slightly aft of the measured, which possibly suggests a difference in source and directivity of the events to the overall waveform energy.

Correlation analysis using cross-correlation coefficients reveals that near-field, crackle-related events are related to far-field measurements. Cross-correlation coefficients, ρ_{xy}, were calculated for the time-aligned propagated and measured waveform segments of 10-ms length centered about each of the 750 events. Spatially, ρ_{xy} values generally decrease with increased distance and are greater for 130° to150° than lower angles. Over half of the events for 130° to 150° have $0.5 > \rho_{xy}$. Relative to the ρ_{xy} for the entire propagated 20.48-s waveform, the median of the distribution for the events is greater, suggesting that the events are among the most correlated portions of the waveform. Example waveforms demonstrated that both near-field shock and large-amplitude pressure events give rise to far-field shocks that are likely related to the perception of crackle. These near-field events are not necessarily source phenomena, as nonlinear propagation may play a role in their propagation from the source to near-field measurement location. In addition, these near-field events may include nonlinear reflections. This all suggests that the near-field events examined are likely related to far-field measures through nonlinear propagation. Further probing towards the source to understand the physical origin of the near-field events is necessary to establish crackle as primarily a propagation phenomenon rather than a source phenomenon. Future investigation into individual events is warranted in order to determine their relationship more fully to far-field crackle perception.

5. ACKNOWLEDGMENTS

The author gratefully acknowledge funding for the measurements provided through the F-35 Program Office and Air Force Research Laboratory. (Distribution A: Approved for public release; distribution unlimited. F-35 PAO Cleared 06/24/2021; JSF20-1006) This research was funded under an Air Force Research Laboratory SBIR program.

6. REFERENCES

[1] J. E. Ffowcs Williams, J. Simson, and V. J. Virchis, " 'Crackle': An annoying component of jet noise," *Journal of Fluid Mechanics*, Vol. 71, No. 2, pp. 251–271 (1975). https://doi.org/10.1017/S0022112075002558

[2] A. Krothapalli, L. Venkatakrishnan, and L. Lourenco, "Crackle: A dominant component of supersonic jet mixing noise," AIAA Paper 2000-2024, June 2000. https://doi.org/10.2514/6.2000-2024

[3] A. B. Vaughn, K. L. Gee, S. H. Swift, K. M. Leete, A. T. Wall, J. M. Downing, and M. M. James, "Source localization of crackle-related events in military aircraft jet noise," *AIAA Journal*, Vol. 59, No. 6, pp. 2251–2261 (2021). https://doi.org/10.2514/1.J059823

[4] A. B. Vaughn, K. M. Leete, K. L. Gee, B. R. Adams, and J. M. Downing, "Evidence for nonlinear reflections in shock-containing noise near high-performance military aircraft," *Journal of the Acoustical Society of America*, Vol. 149, No. 4, pp. 2403–2414 (2021). https://doi.org/10.1121/10.0003932

[5] K. L. Gee, P. B. Russavage, T. B. Neilsen, S. H. Swift, and A. B. Vaughn, "Subjective rating of the jet noise crackle percept," *Journal of the Acoustical Society of America*, Vol. 144, No. 1, EL40–EL44 (2018). https://doi.org/10.1121/1.5046094

[6] K. L. Gee, T. B. Neilsen, J. M. Downing, M. M. James, R. L. McKinley, R. C. McKinley, and A. T. Wall, "Near-field shock formation in noise propagation from a high-power jet aircraft," *Journal of the Acoustical Society of America*, Vol. 133, No. 2, EL88–EL93 (2013). https://doi.org/10.1121/1.4773225

[7] B. O. Reichman, K. L. Gee, T. B. Neilsen, and S. H. Swift, "Acoustic shock formation in noise propagation during ground run-up operations of military aircraft," AIAA Paper 2017-4043, June 2017. https://doi.org/10.2514/6.2017-4043

[8] K. L. Gee, T. B. Neilsen, M. B. Muhlestein, A. T. Wall, J. M. Downing, M. M. James, and R. L. McKinley, "On the evolution of crackle in jet noise from high-performance engines," AIAA Paper 2013-2190, June 2013. https://doi.org/10:2514/6.2013-2190

[9] K. L. Gee, T. B. Neilsen, A. T. Wall, J. M. Downing, M. M. James, and R. L. McKinley, "Propagation of crackle-containing jet noise from high-performance engines," *Noise Control Engineering Journal*, Vol. 64, No. 1, pp. 1–12 (2016). https://doi.org/10.3397/1/376354

[10] C. L. Morfey and G. P Howell, "Nonlinear propagation of aircraft noise in the atmosphere," *AIAA Journal*, Vol 19, No. 8, pp. 986–992 (1981). https://doi.org/10.2514/3.51026

[11] K. L. Gee, T. B. Gabrielson, A. A. Atchley, and V. W. Sparrow, "Preliminary analysis of nonlinearity in military jet aircraft noise propagation," *AIAA Journal*, Vol. 43, No. 6, pp. 1398–1401 (2005). https://doi.org/10.2514/1.10155

[12] K. L. Gee, V. W. Sparrow, M. M. James, J. M. Downing, C. M. Hobs, T. B. Gabrielson, and A. A. Atchley, "The role of nonlinear effects in the propagation of noise from high power aircraft," *Journal of the Acoustical Society of America*, Vol. 123, No. 6, pp. 4082–4093 (2008). https://doi.org/10.1121/1.2903871

[13] K. L. Gee, J. M. Downing, M. M. James, R. C. McKinley, R. L. McKinley, T. B. Neilsen, and A. T. Wall, "Nonlinear evolution of noise from a military aircraft during ground run-up," AIAA Paper 2012-2258, June 2012. https://doi.org/10:2514/6.2012-2258

[14] B. O. Reichman, M. B. Muhlestein, K. L. Gee, T. B. Neilsen, and D. C. Thomas, "Evolution of the derivative skewness for nonlinearly propagating waves," *Journal of the Acoustical Society of America*, Vol. 139, No. 3, pp. 1390–1403 (2016). https://doi.org/10.1121/1.4944036

[15] M. B. Muhlestein, K. L. Gee, T. B. Neilsen, and D. C. Thomas, "Prediction of nonlinear propagation of noise from a solid rocket motor," *Proceedings of Meetings on Acoustics*, Vol. 18, No. 1 040006 (2013). https://doi.org/10.1121/1.4828827

[16] B. M. Harker, T. B. Neilsen, K. L. Gee, A. T. Wall, and M. M. James, "Spatiotemporal-correlation analysis of jet noise from a high-performance military aircraft," *AIAA Journal*, Vol. 54, No. 5, pp. 1554–1566 (2016). https://doi.org/10.2514/1.J054442

[17] K. Viswanathan, J. R. Underbrink, and L. Brusniak, "Space-time correlation measurements in near fields of jets," *AIAA Journal*, Vol. 49, No. 8, 1577–1599 (2011). https://doi.org/10.2514/1.J050750

[18] C. K. W. Tam, N. N. Pastouchenko, K. Viswanathan, "Continuation of the near acoustic field of a jet to the far field part I: theory," AIAA Paper 2010-3728, June 2010. https://doi.org/10.2514/6.2010-3728

[19] C. K. W. Tam, K. Viswanathan, N. N. Pastouchenko, and B. Tam, "Continuation of near-acoustic fields of jets to the far field part II: experimental validation and noise source characteristics," AIAA Paper 2010-3729, June 2010. https://doi.org/10.2514/6.2010-3729

[20] M. M. James, A. R. Salton, J. M. Donwing, K. L. Gee, T. B. Neilsen, B. O. Reichman, R. L. McKinley, A. T. Wall, and H. L. Gallagher, "Acoustic emissions from F-35 aircraft during ground run-up," AIAA Paper 2015-2375, June 2015. https://doi.org/10.2514/6.2015-2375

[21] F. M. Pestorius and D. T. Blacksotck, "Propagation of finite-amplitude noise," in *Finite-Amplitude Wave Effects in Fluids*, edited by L. Bjorno (IPC Science and Technology, Guildford, 1973), pp. 24–29 (1973).

[22] M. O. Anderson, "The propagation of a spherical N wave in an absorbing medium and its diffraction by a circular aperture," Technical Report No. ARL-TR-74-25, Applied Research Laboratories, The University of Texas at Austin, Austin, TX (1974).

[23] K. L. Gee, "Prediction of nonlinear jet noise propagation," Ph.D. thesis, The Pennsylvania State University, University Park, PA (2005).

[24] P. B. Russavage, T. B. Neilsen, K. L. Gee, K.L. and S. H. Swift, "Rating the perception of jet noise crackle." *Proceedings of Meetings on Acoustics*, Vol. 33, No. 1, p. 040001 (2018). https://doi.org/10.1121/2.0000821